Boron-induced Metamorphosis on Graphitic Structures - A new form of mesoscopic carbon

Elena Echeverria, Aaron J. Austin, Nate Dice, A. Kaan Kalkan, Linqi Zhang, Binbin Weng, Derek Meyer, David N. McIlroy

PII: \$2667-0569(20)30012-2

DOI: https://doi.org/10.1016/j.cartre.2020.100012

Reference: CARTRE 100012

To appear in: Carbon Trends

Received date: 3 November 2020 Revised date: 20 November 2020 Accepted date: 25 November 2020



Please cite this article as: Elena Echeverria, Aaron J. Austin, Nate Dice, A. Kaan Kalkan, Linqi Zhang, Binbin Weng, Derek Meyer, David N. Mcllroy, Boron-induced Metamorphosis on Graphitic Structures - A new form of mesoscopic carbon, *Carbon Trends* (2020), doi: https://doi.org/10.1016/j.cartre.2020.100012

This is a PDF file of an article that has undergone enhancements after acceptance, such as the addition of a cover page and metadata, and formatting for readability, but it is not yet the definitive version of record. This version will undergo additional copyediting, typesetting and review before it is published in its final form, but we are providing this version to give early visibility of the article. Please note that, during the production process, errors may be discovered which could affect the content, and all legal disclaimers that apply to the journal pertain.

© 2020 Published by Elsevier Ltd. This is an open access article under the CC BY-NC-ND license (http://creativecommons.org/licenses/by-nc-nd/4.0/)

HIGHLIGHTS

- New tubular mesoscopic carbon structures that are not related to well-known CNT
- Metamorphosis of carbon induced due to boron inclusion
- Hollow filamentary carbon structures grown by a metal-free APCVD process
- Use of dopants to predetermine the morphology of carbon materials
- Inversion of the curvature of carbon hemispheres due to doping-induced strain



Boron-induced Metamorphosis on Graphitic Structures - A new form of mesoscopic carbon

Elena Echeverria^{1,*}, Aaron J. Austin¹, Nate Dice¹, A. Kaan Kalkan², Linqi Zhang², Binbin Weng³, Derek Meyer¹, and David N. Mcllroy¹

SUMMARY

Several new allotropes of carbon have been discovered in recent decades with unique physical properties, enabling innovations in numerous applications from energy storage/conversion to water purification to drug delivery. The exceptional versatility of carbon begs the question, are there other carbon allotropes or mesoscale structures yet to be discovered? Herein, a unique mesoscopic tubular carbon is introduced, referred to as Boron Ortho-carborane Doped (BOD) Carbon, which is obtained by boron doping of the pseudo-graphite known as GUITAR (Graphite University of Idaho Tar). BOD-carbon exhibits a disordered nano-graphitic structure with basal atomic planes aligned with the tube axis. While GUITAR consists of overlapping downward curving structures, BOD-

¹ Department of Physics, Oklahoma State University, Stillwater, QK 74078-3072, United States

² School of Mechanical and Aerospace Engineering, Oklahoma State University, Stillwater, OK 74078, United States

³ School of Electrical and Computer Engineering, University of Oklahoma, Norman, OK 73019, United States

^{*} Corresponding author: Tel: 405 744 7478. E-mail: elena.echeverria@okstate.edu (Elena Echeverria)

carbon consists of upward-curving hemispheres. The change in the growth direction characteristic of BOD-carbon as well as its two-stage growth from spherical to tubular, are attributed to B substitution of C and/or interstitial B, concomitant with a different strain state that modifies the energy in C—C bonds as well as at the carbon-Si interface. This work demonstrates that previously unobserved forms of graphitic carbon can be obtained by manipulating strain in graphitic carbon at the atomic scale. BOD-carbon promises unique applications beyond the capabilities of the already known carbon nanotubes.

Keywords: Graphitic, carbon, GUITAR, boron, mesostructures

1. INTRODUCTION

It is widely known that the properties of carbon-based materials are highly dependent on their morphology and carbon bonding, i.e., sp², sp³, or a mixture thereof. For example, graphite with sp² bonding is conductive, while diamond with sp³ bonding is a wide bandgap insulator.

Similarly, the chirality of a carbon nanotube and/or its geometrical structure determines whether it will be a semiconductor or a conductor^{1–7}. Recently, superconducting carbon has been realized with misaligned graphene layers⁸. Furthermore, different carbon allotropes have unique properties that enable carbon to be used in a wide variety of innovative applications, such as energy storage media^{9,10}. While graphite is one of the materials of choice for Li-ion batteries, fast charging can lead to swelling and flaking¹¹ or breaking of the graphite particles into smaller particles¹², which diminishes its storage capacity or cycle life or leads to catastrophic failure^{13,14}. However, it has also been shown that some of these adverse effects can be alleviated by modifying the morphology of the carbon allotrope^{15–17} or incorporating carbon and another

(other) element(s) into a hybrid structure¹⁸ or through fabrication techniques that protect the graphite anode¹⁹.

All of these examples show that the road to the discovery of new and novel forms of carbon is through the development of new techniques for simultaneously manipulating its bonding and the morphology of the structures produced. In this direction, our group has found that it is possible to control the morphology of a graphitic carbon by the introduction of strain into its graphitic lattice. Herein, we introduce a method for controlling the morphology of graphitic carbon by modifying the bonding, and subsequently the strain within nanographite, through the incorporation of boron into the graphite lattice. We report on the successful use of boron doping to produce a new tubular morphology of carbon, which hereon will be referred to as Boron Orthocarborane Doped Carbon or BOD-carbon. The process for producing BOD-carbon is based on an atmospheric pressure chemical vapor deposition (APCVD) process developed by Cheng et al.^{20–26} to produce a pseudo-carbon known as GUITAR (Graphite from the University of Idaho Tar). Due to its unique electrochemical properties^{20,22,27}, GUITAR, in comparison to regular graphite, is a more favorable choice in applications such as sensors²⁵, energy storage and conversion²⁴, and water purification²⁸.

Previous experiments on the effects of doping of carbon-based nanostructures ^{1,7,29–31} have primarily observed enhancement of a specific property of the material, as opposed to morphological changes. Doping also has the effect of changing carbon-based materials from being a conductor to a semiconductor ^{1,3,5,6}. The exception is nitrogen doping of carbon nanotubes (CNT) ^{2,7,31,32}, where morphological changes produce bamboo-like formations or curling of the CNT. These morphological changes are typically accompanied by changes to their electrical conductivity ^{3,4,7,30,33} due to distortions of the graphene lattice.

The intended goal of doping GUITAR with boron was to create or increase sp³ bonding, and with sufficient inclusion of boron, transform GUITAR into boron carbide (B₄C) or produce regions of B₄C within GUITAR. The processes typically used to synthesize boron carbide results in low charge carrier diffusion coefficient³⁴, low fracture toughness and/or oxidation resistance³⁵. Therefore, growing enhanced boron carbide-based materials that have the unique properties of the GUITAR would be highly desirable.

Herein, we introduce a method for controlling the morphology of graphitic carbon by modifying the strain within nanographite, through the incorporation of boron into the graphite lattice. The novelty of this approach is that B is doped *in-situ* with no need of a metal catalyst. As a result, new and novel carbon structures can be produced, as well as providing new insight into the use of dopants to predetermine the morphology of carbon materials.

2. BORON ORTHO-CARBORANE DOPED (BOD) CARBON MORPHOLOGY

While B-doping of graphitic materials is known to modify their electrochemical and optical properties ^{1,5,10,32,36–38}, significant changes to their morphology have not been reported.

Surprisingly, this is not the case with GUITAR, even though it is a nanographitic material. As we will show, the morphology of undoped GUITAR lends itself to the formation of the structures reported herein when B is incorporated into the graphitic structure. Displayed in Figure 1 is a montage of scanning electron micrographs of BOD-carbon grown for one hour at 900 °C on a Si substrate. At low magnification (Fig. 1a), BOD-carbon appears to be a medium density array of carbon filamentary structures. Closer examination reveals that the filaments range in length from ~9-20 μm and are open-ended (Fig. 1b), however, the ends of some do taper down, or occasionally, completely close. The medium resolution top-down view reveals the hollow nature of the structures (Fig. 1c). The high-resolution SEM image in Fig. 1d reveals that the BOD-

carbon structures are microns across and have extremely thick walls in the range of 50-100 nm. The dimensions of the BOD-carbon filaments far exceed those reported for large diameter CNT^{39-42} or multiwalled CNT^{43-46} . The atomic concentration of B in BOD-carbon in this study has been determined to be 3.0 ± 0.6 % based on X-ray photoelectron spectroscopic (XPS) analysis (See supporting information for more details, Figure S1).

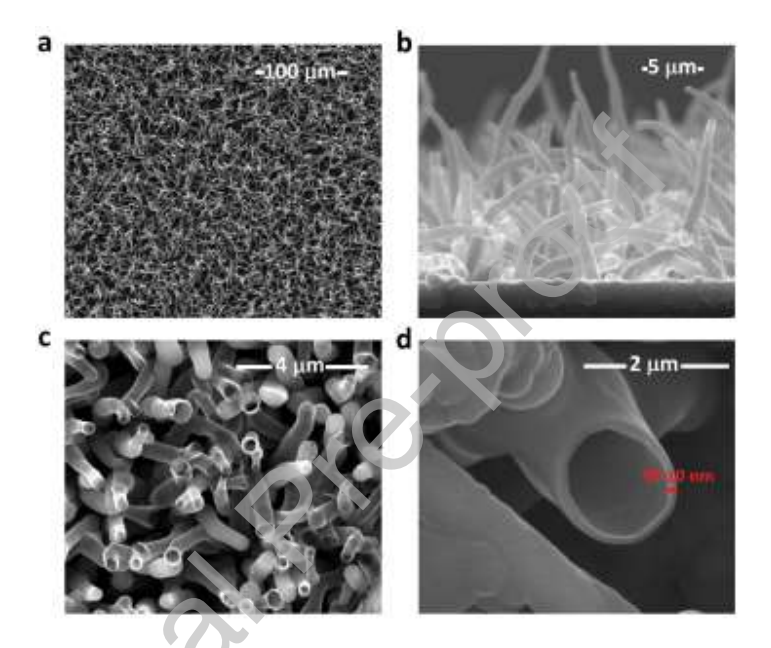


Figure 1. **Images of the BOD-carbon structures. a,b,** Scanning Electron Microscopy (SEM) image for an ensemble of tubular BOD-carbon top and side view of the structures clearly showing large area covering. **c,** High magnification images of the tubular BOD-carbon. **d,** a close up of a single BOD-carbon opening showcasing the thickness of the wall.

To further confirm that boron is present only in the BOD-carbon structures, energy dispersive X-Ray Spectroscopy (EDS) measurements were taken on a sample where the structures did not completely cover the wafer (see Figure S2a). Two localized areas were studied: region 1 with a bundle of tubular BOD-carbon and region 2 with no structures, i.e. pure GUITAR. EDS spectra show B, C, O and Si peaks in region 1 while only C, O and Si peaks are seen in region 2 (See

Figure S2b and S2c). Therefore, the conclusion is that boron is needed to form the new BOD-carbon morphology.

Transmission electron micrographs (TEM) of the BOD-carbon filaments (Fig. 2a-2b) confirm that they are indeed hollow. The BOD-carbon filaments do not exhibit the bamboo-like morphology characteristic of MWCNT structures ^{47,48} and, therefore, are not a member of this family of materials and, thus, exhibit a new mesoscopic morphology of carbon. High magnification TEM images (Figure 2c-2d) of the wall of an individual BOD-carbon filament show that the wall is composed of disordered layers of nanographite, similar to the structure of GUITAR²⁷. The graphitic layering of the filaments is likely why they are hollow, as opposed to solid carbon microfibers. The similarities between the microstructure of BOD-carbon and GUITAR suggest that the inclusion of B and subsequent formation of tubular carbon cannot be attributed simply to a higher degree of disorder of the layered structure of GUITAR, but instead, B inclusion affects bonding within the graphite layers and bonding between graphite layers. One can see from a closer examination of TEM images in panels (a) and (b) of Fig. 2 that there are three types of terminations of the BOD-carbon filaments – flared outward, straight, or closed. In nearly all cases, the inner diameter of the filament increases, while the outer diameter for the most part remains constant. This is most apparent in panel (b) in Fig. 2 of a closed-ended filament. We suggest that this is a result of strain associated with B inclusion in and at the edges of the graphite sheets within the BOD-carbon filament and critical to understanding their formation. A selected area diffraction (SAD) patter (See Figure S3) indicates that BOD-carbon is a polycrystalline form of carbon with an interlayer spacing of 0.45 nm. While this is close to the interlayer spacing for graphite oxide^{49–52}, X-ray photoelectron spectroscopic analysis and Raman spectroscopy (Figure S4) of BOD-carbon do not correlate with graphite oxide.

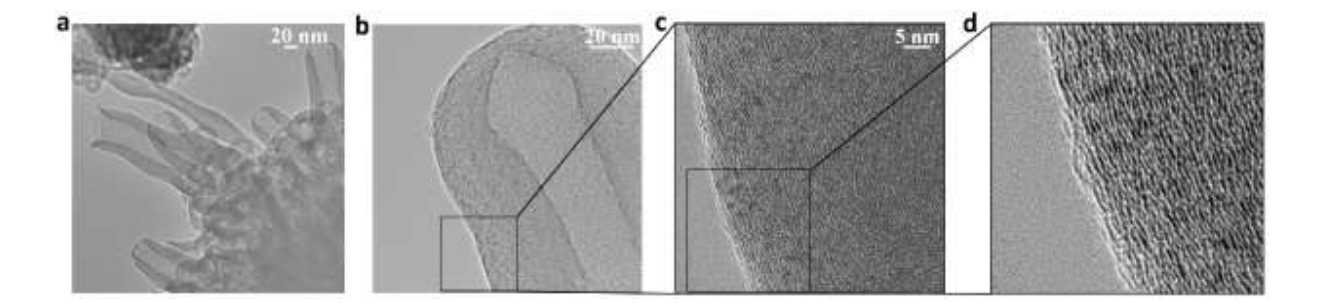


Figure 2 Evidence of a layered but disordered graphitic structure. a,b, Transmission Electron Microscopy (TEM) images of a bundle of tubular BOD-carbon and a tip of a closed tubular BOD carbon. c,d, High magnification images of the side of a BOD-carbon tubular structure.

3. BOD-CARBON NUCLEATION AND FORMATION

To understand how B doping alters/impacts the GUITAR process and, ultimately, leads to the formation of BOD-carbon tubular filaments, we must develop growth models for both GUITAR and BOD-carbon. In the original GUITAR process^{20,21,23}, sulfur (S) facilitates carbon nucleation by dissociating CO, CO₂, and hydrocarbons and carrying away O and H in the form of SO₂ and H₂S, respectively. In other words, S serves as a promotor for the rapid formation of GUITAR. Typically, the initiation of GUITAR formation is the emergence of a yellow vapor from the exhaust end of the tube furnace. Note that S is used in the vulcanization of rubber^{53,54}, where it promotes crosslinking. We believe that it serves the same purpose in the GUITAR process^{20,21,23}. While GUITAR has a layered structure that exfoliates, unlike graphite, the thickness of the exfoliated layers is on the order of microns²⁰. Furthermore, the microstructure of GUITAR is an agglomeration of carbon hemispheres ~50-100 nm in diameter²⁷.

We begin by examining the initial phases of the growth of BOD-carbon. Displayed in Figure 3a is an SEM of a typical BOD-carbon filament that is analogous to a hair with the follicle attached.

The initial growth can best be described as an ellipsoidal structure (follicle) from which the tubular structure (hair) emerges. The inner core of the follicle can be observed with SEM in the fortuitous case where the tube has separated just above the follicle. One such example is displayed in Fig. 3b. The follicle consists of an inner closed core (highlighted in blue) and an outer wall that continues to grow to form the walls of the BOD-carbon filament. While not a topic of this report, the length and wall thickness of the BOD-carbon filaments depends on the growth time and the ratios of the boron precursor to the carbon precursor to sulfur in the bubbler.

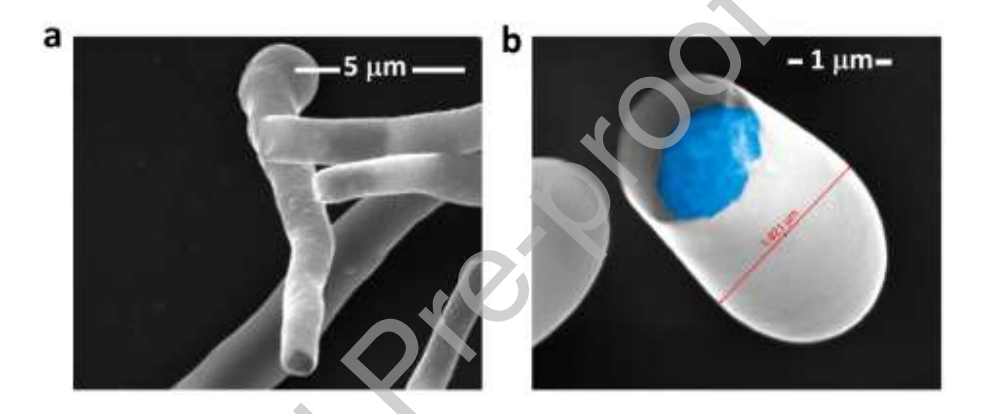


Figure 3. **Stages of the BOD carbon formation. a,b,** High magnification SEM images of a BOD carbon structure at the completely formed and early stage.

To better understand the formation of BOD-carbon, atomic force microscope (AFM) mapping of the backside of delaminated films of GUITAR and BOD-carbon have been carried out and displayed in Figure 4. In the case of GUITAR, the backside of the film is relatively smooth except for some circular pits (Fig. 4a). The RMS roughness of the backside of GUITAR is 0.3 nm in the pit free regions and the average diameter of the pits is 58 ± 12 nm. In contrast, AFM mapping of the backside of the delaminated films of BOD-carbon (Fig. 4b) reveals an extremely rough surface consisting of clusters of hemispherical bumps, reminiscent of the top surface of

GUITAR, with an RMS roughness of 8.5 nm or 28 times rougher than the backside of GUITAR. The average diameter of the bumps is 105 ± 15 nm.

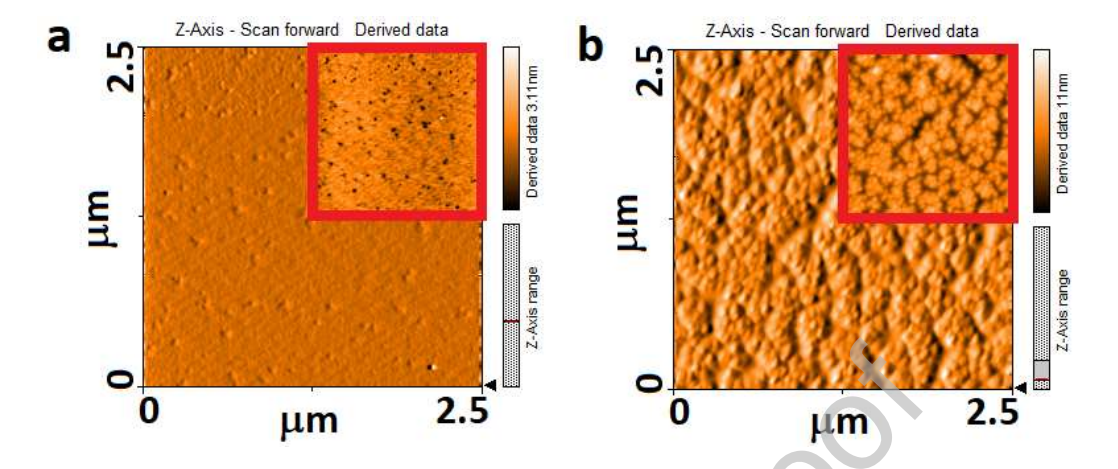


Figure 4. Surface morphology of GUITAR and BOD-carbon. a,b, Atomic Force Microscope (AFM) images for GUITAR and BOD carbon. The top corners on each image show the line analysis for each image.

4. DISCUSSION

It is the opinion of the authors that the dramatic change in the morphology of GUITAR with B-doping is not concomitant with a dramatic change in the growth mechanism of GUITAR but, instead, is a consequence of B-induced strain of the hexagonal sp² bonded carbon lattice and disorder associated with increased sp³ bonded carbon. Consequently, a modification of a model of the formation of GUITAR is the starting point for developing a model for BOD-carbon. We will present a model of GUITAR formation and then expand this model to include the effects of B-doping and the resulting BOD-carbon morphology.

The morphology of the top surface of GUITAR is best described as an agglomeration of carbon micro-hemispheres with diameters ranging from tens to hundreds of nanometers²⁷. The graphite hemispheres or carbon onion structures^{48,55}, as some have described them, form one atop another,

where AFM images of the top surface are reminiscent of the AFM of the backside of released BOD-carbon in Fig. 4b. We postulate that the pits or voids in the AFM image of the backside of released GUITAR in Fig. 4a are the unfilled centers of the graphite hemispheres forming GUITAR, where not all of the hemispheres possess these voids. Our model of the formation of the graphite hemispheres of GUITAR is schematically presented in Figure 5. Avogadro software ⁵⁶ was used to construct and calculate the ground state energies of a large and small freestanding flat graphene sheets, and lastly, a graphite hemisphere, as expected from the formation of the hemispheres in GUITAR²⁷. Interactions between the graphene sheets and the substrate or between sheets have not been included in this calculation but having simulations on the graphene planes can give us a basic idea of what to expect after doping.

As expected, the smaller flat sheet of graphene is the lowest energy state and energetically favored over the curved sheet. We postulate that the interface interaction significantly lowers the ground state energy of the curved graphene sheet, such that it is the favorable microstructure of GUITAR. While not a topic of this work, sulfur may affect the interface dynamics/energy and further enhance the curvature of the graphene sheets by accelerating the growth of GUITAR, which results in defects that distort the lattice and leads to strain.

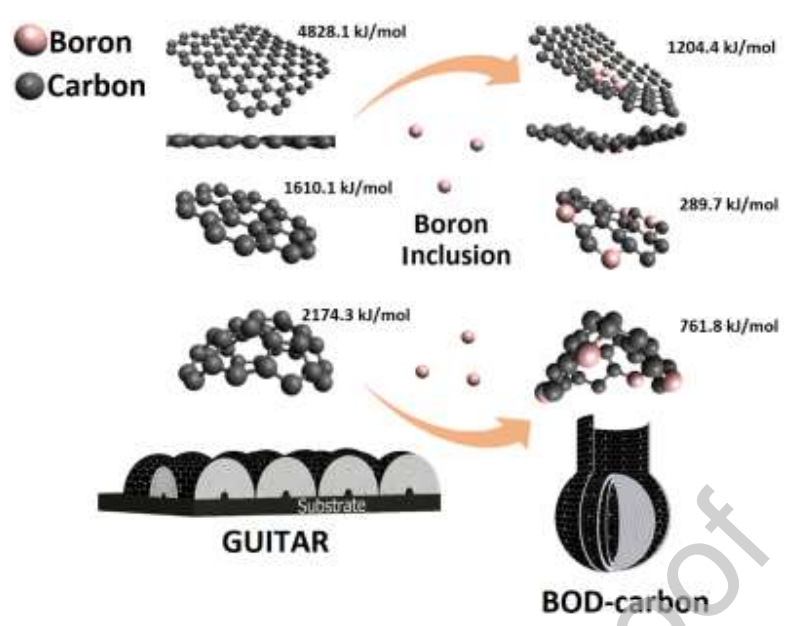


Figure 5. **Modeling the B incorporation into the carbon lattice.** Three different models for a carbon lattice (on the left) and how these are affected by B inclusion (structures on the right). Total energies are included on top of each model. Bottom of the image shows a schematic representation of the onion-like structure for GUITAR (bottom left) and the tubular formation for BOD carbon (Bottom right).

Raman spectroscopy can provide important information about strain in graphitic materials based on the position of the D and G bands. The Raman D and G bands of GUITAR are at 1355 and 1601 cm⁻¹, respectively, and the ratio of the band intensities, I(D)/I(G), is 0.91, which is consistent with the value reported in the GUITAR literature^{20,22,23,57}. The fact that the position of the G band of GUITAR²⁷ is closer to that of a single-wall carbon nanotube than graphene^{58,59} implies that the nanographite sheets of graphitic hemispheres are strained due to their curved morphology and consistent with the model in Figure 5.

Based on the above model for GUITAR, we have concluded that B doping of GUITAR modifies the strain within the graphite hemispheres and that this drives the filamentary morphology of BOD-carbon. To support this conclusion, we have modeled the inclusion of B within a carbon lattice and corresponding lattice distortions. The lowest energy state of graphene with B substituted for C has been recalculated with Avogadro and the corresponding geometry

determined. The results of the calculation are presented on the right side of Figure 5. Boron substitution significantly reduces the energy of the lowest energy state of all three geometries calculated for graphene on the left side of Figure 5. In the case of the two flat graphene structures, the lowering of the energy of the system is achieved by a distortion of the lattice and a corresponding curvature of the graphene sheet. In the case of the already curved graphene sheet, B inclusion alone does not invert its curvature, but the interaction between planes will do so due to the crosslinking between layers facilitated by the increase of sp³ carbon bonds^{30,60}. It is already known that B introduces in-plane structural strain in mesocarbon microbeads⁶¹ and that B substitution slightly deforms layers on highly oriented pyrolytic graphite (HOPG)³⁶. In the context of GUITAR, B-doping will produce an upward curving morphology relative to the substrate, which is due to the additional strain out of plane or between planes generated by the sp³ carbon sites. The Raman spectrum of BOD-carbon supports the conclusion of B induced strain. Specifically, the G band of BOD-carbon is at 1593 cm⁻¹, a downshift of 8 cm⁻¹ relative to GUITAR. Corro et al. 59 have shown that tensile strain produces a shift of the G band of graphite and graphene related materials. The position of the D band of BOD-carbon is at the same wavenumber as GUITAR, however, the ratio of the intensities of the D and G bands, I(D)/I(G), is 0.97, as compared to 0.91 for GUITAR (See Figure S4). The increase of I(D)/I(G) of BODcarbon is attributed to increased disorder relative to GUITAR and a concomitant increase in sp³ bonding. This conclusion is further supported by X-ray photoelectron spectroscopy of GUITAR and BOD-carbon. For undoped GUITAR, the C 1s core level peak consists of a primary peak at a binding energy of 284.6 eV that is associated with sp² bonding and an asymmetric tail that is characteristic of carbon with high concentrations of sp² bonding ⁶². For BOD-carbon, the primary

C 1s core level peak is at a lower binding energy of 284.0 eV, where this shift is associated with the formation of C-B bonds^{62–64}.

Based on the SEM and TEM micrographs, Raman and XPS spectroscopies, and the literature, we have developed a model of BOD-carbon filament formation based on B-induced strain of the graphitic carbon lattice. The model is summarized in the bottom two illustrations in Figure 5. Simply stated, tensile strain within the graphene sheets forming the nanographite of BOD-carbon flips the direction of curvature of the GUITAR carbon hemispheres, such that the growth direction is now normal to the substrate. This is supported by the reduction of the Raman G band of BOD-carbon relative to GUITAR, which corresponds to tensile strain⁵⁹, and modeling of the effect of B-doping of the graphene lattice. As a consequence of the growth normal to the substrate, the carbon hemispheres of GUITAR continue to grow. However, because of the tensile strain, the carbon hemispheres attempt to close. The radius of the inner core of the hemisphere can accomplish this feat, where we hypothesize that this is due to the combination of the tensile stress and the Van der Waals attraction between graphene sheets. However, at larger radii, the tensile stress and the Van der Waals attraction is insufficient, and the outer layers of the carbon hemisphere decouple from the inner core and, instead, continue to grow vertically to form the tubular filament. The closed core and ellipsoidal follicle that tapers before the hollow filament forms in Figure 3 supports the model. The strength of the model is its simplicity and that it incorporates known phenomena of carbon formation. More importantly, it suggests that strain can be utilized as a growth parameter for designing macroscopic forms of carbon with attributes specific to a proposed application.

5. OUTLOOK

While BOD-carbon filaments are hollow like well-known CNT, they are significantly different and, therefore, are amenable for use in applications that are beyond the capabilities of CNT. The ability of only 3% of B doping to completely invert the curvature of the carbon hemispheres of GUITAR and create macroscopic hollow tubular structures compels one to consider the possibility of creating macroscopic carbon structures that have attributes of nanographite and the free space within that can readily be filled with any manner of material. Furthermore, utilizing doping-induced strain as a tool for designing macroscopic carbon. Note that the observed phenomenon is unlikely to translate to the nanoscale due to the relative strength of Van der Waals forces at this scale.

Although past research has shown that B doping of graphene speeds up Li diffusion through sheets and enhances battery capacity^{65,66}, we believe that if diffusion through the walls of the BOD-carbon is possible, there are clear advantages to using this material in a Li-Ion battery electrodes and hydrogen absorption. It has already been demonstrated that B doping of graphite dramatically increases hydrogen absorption⁶⁷, but the hollow nature of BOD-carbon allows hydrogen to absorb into the inner and outer walls, thereby increasing absorption/desorption rates and capacity. Depending on the B concentration, H will absorb preferentially near B atoms and promote the formation of H clusters⁶⁸. Thus, controlling B content will allow us to tune the H absorption of this material. BOD-carbon undoubtedly has the potential to improve energy storage and hydrogen absorption technologies.

It has also been shown that B inclusion reduces the oxidation of the carbon at high temperatures^{29,37}, therefore, protecting structures from corrosion. Also, the fact that these new structures are mesoscopic and hollow makes them suitable for various applications requiring large surface areas, as previously mentioned. As for drug delivery and water purification with

BOD-carbon, further research is needed, however, since a metal catalyst is not used in the growth process, there is promise that this will reduce their toxicity.

This all alludes to the tunability of these structures, and subsequent other morphologies, whereby controlling the B content one can cater the morphology to specific applications. As stated beforehand, B concentration matters for many different applications therefore careful engineering of this could indeed lead to a favorable material. Although the results presented here represent research quantities grown on Si wafers, BOD-carbon can be grown on other substrates and without planar surfaces, i.e. substrate independent growth. This supports the conclusion that growth is primarily driven by the relative ratios of the precursors, growth time, and the APCVD process. This is a desirable attribute that will enable BOD-carbon to be utilized in a broad range of applications.

Further exploration of the BOD-carbon process is the key to unlocking the full potential of the GUITAR process in conjunction with doping, be it B, N, etc. Consequently, ongoing studies continue to further elucidate the subtle effects of B-doping on the GUITAR process and subsequent electrical and chemical properties of BOD-carbon.

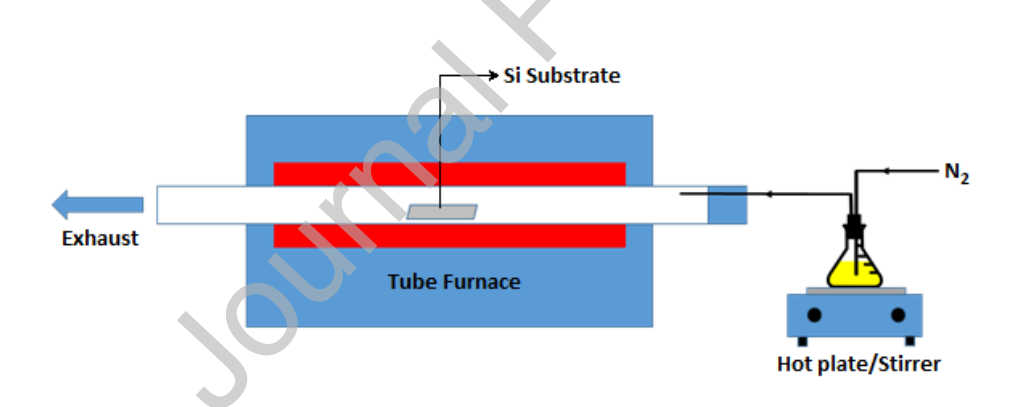
6. METHODS

6.1 Samples Preparation

Boron ortho-carborane doped (BOD) carbon mesoscopic structures were synthesized on RCA cleaned Si substrates by atmospheric pressure chemical vapor deposition (APCVD). A schematic of the APCVD system is shown in Extended Data Figure 1. The system consists of a horizontal tube furnace (Thermo Scientific Lindberg/Blue M), a quartz tube that serves as the reactor, a hot plate/stirrer (Corning), and a bubbler. Different quantities of ortho-carborane (Katchem) and sulfur (Fisher Scientific) were added to 100 mL 99 wt% cyclohexanol (Sigma Aldrich) to obtain

different mesoscopic morphologies. The mixture B/sulfur/cyclohexanol was heated and magnetically stirred during the entire process. Substrates on a ceramic boat were placed in the hot zone of the furnace and the furnace temperature was ramped up under a constant flow of N₂. N2 was also used as the precursor carrier gas. The furnace was heated to 900 °C and solution to about 120 °C and maintained during the growth process. Deposition times ranged from 10 min to 1 h, where the clock started once the furnace reached 900 °C. The reactor tube was cleaned prior to each growth.

The APCVD process involves the pyrolysis of a material with a large molar fraction of carbon in the presence of sulfur. Sulfur acts as a promoter of carbon nucleation in the APCVD process that allows one to produce reasonable quantities of GUITAR in a short amount of time, which makes this technique very attractive.



Extended Data Figure 1. **CVD method used for growing samples.** A schematic of the chemical vapor deposition system (CVD) used to grow the BOD nanostructures.

6.2 Characterization

An EI Quanta 600 Field Emission Scanning Electron Microscopy (FESEM) equipped with a Bruker EDS and HKL EBSD was used to acquire micrographs of the samples. Double-sided carbon tape was used to mount the samples to the FESEM sample posts. Transmission Electron Microscopy (TEM) micrographs were acquired with a JEOL JEM-2100 with Bruker EDS.

Atomic Force Microscopy (AFM) measurements were performed with a Nanosurf Easyscan 2.

Both GUITAR and BOD carbon samples were exfoliated with scotch tape. X-Ray photoelectron spectroscopy (XPS) was performed in an ultra-high vacuum system (UHV) with a base pressure of 6.0 x 10⁻¹⁰ Torr. The XPS spectra were acquired using the Al-Kα emission line from a dual anode X-ray source (Physical Electronics XR 04-548) operated at 400 W and an incident angle of 54.7°. Raman spectra were acquired by a WITec alpha300 micro-Raman system, equipped with a 532 nm excitation laser. The signal was accumulated for 200 s employing an 1800 lines/mm grating, 20× objective lens, incident laser power of 2.5 mW, and laser spot of 10 μm diameter. The BOD-carbon Raman peaks exhibited photothermal shifts above an incident laser power of 3 mW. Therefore, the acquisitions were performed at 2.5 mW incident power for both GUITAR and BOD-carbon samples.

Declaration of Competing Interest

The authors declare that they have no known competing financial interests or personal relationships that could have appeared to influence the work reported in this paper.

ACKNOWLEDGEMENTS

DMc would like to acknowledge the support of the Office of Naval Research (N00014-20-1-2433). A.K.K. acknowledges the funding by National Science Foundation (Award #1707008).

E.E. acknowledges Dr. J. Monroy for his assistance with the diagrams of GUITAR and BOD schematics.

AUTHOR CONTRIBUTIONS

E.E., A.A. and D.Mc. conceived the idea, designed the experiments, collected the data and wrote the manuscript. N.D. and D.M. assisted collecting and analyzing the AFM data. A.K.K., L.Z. and B.W. assisted collecting and analyzing the RAMAN data.

ADDITIONAL INFORMATION

Correspondence and material requests should be addressed to EE

REFERENCES

- Ma, J., Guan, S. & Lai, C.-H. Disorder effect on electronic and optical properties of doped carbon nanotubes. *Phys. Rev. B* 74, 205401 (2006).
- 2. Ewels, C. P. & Glerup, M. Nitrogen Doping in Carbon Nanotubes. *J. Nanosci. Nanotech.* **5**, 1345–1363 (2005).
- 3. Rao, C. N. R., Gopalakrishnan, K. & Govindaraj, A. Synthesis, properties and applications of graphene doped with boron, nitrogen and other elements. *Nano Today* **9**, 324–343 (2014).
- 4. Mousavi, H. & Moradian, R. Nitrogen and boron doping effects on the electrical conductivity of graphene and nanotube. *Solid State Sciences* **13**, 1459–1464 (2011).

- 5. Rani, P. & Jindal, V. K. Designing band gap of graphene by B and N dopant atoms. *RSC Adv.* **3**, 802–812 (2013).
- 6. Gao, S. *et al.* Density functional theory prediction for diffusion of lithium on boron-doped graphene surface. *Applied Surface Science* **257**, 7443–7446 (2011).
- 7. Panchakarla, L. S., Govindaraj, A. & Rao, C. N. R. Boron- and nitrogen-doped carbon nanotubes and graphene. *Inorganica Chimica Acta* **363**, 4163–4174 (2010).
- Cao, Y. et al. Unconventional superconductivity in magic-angle graphene superlattices. Nature 556, 43–50 (2018).
- 9. Mao, M. et al. Pipe-Wire TiO ₂ –Sn@Carbon Nanofibers Paper Anodes for Lithium and Sodium Ion Batteries. *Nano Lett.* **17**, 3830–3836 (2017).
- 10. Romanos, J. *et al.* Infrared study of boron–carbon chemical bonds in boron-doped activated carbon. *Carbon* **54**, 208–214 (2013).
- 11. Aurbach, D. A short review of failure mechanisms of lithium metal and lithiated graphite anodes in liquid electrolyte solutions. *Solid State Ionics* **148**, 405–416 (2002).
- 12. Dose, W. M. *et al.* Capacity fade in high energy silicon-graphite electrodes for lithium-ion batteries. *Chem. Commun.* **54**, 3586–3589 (2018).
- 13. Takahashi, K. & Srinivasan, V. Examination of Graphite Particle Cracking as a Failure Mode in Lithium-Ion Batteries: A Model-Experimental Study. *J. Electrochem. Soc.* **162**, A635 (2015).
- 14. Pender, J. P. et al. Electrode Degradation in Lithium-Ion Batteries. ACS Nano 14, 1243–1295 (2020).
- 15. Roberts, A. D., Li, X. & Zhang, H. Porous carbon spheres and monoliths: morphology control, pore size tuning and their applications as Li-ion battery anode materials. *Chem. Soc. Rev.* **43**, 4341–4356 (2014).
- Tang, K. et al. Hollow Carbon Nanospheres with Superior Rate Capability for Sodium-Based Batteries. Adv. Energy Mater. 2, 873–877 (2012).

- 17. Wang, J. et al. An Advanced MoS $_2$ /Carbon Anode for High-Performance Sodium-Ion Batteries. Small 11, 473–481 (2015).
- 18. Krause, L. J., Brandt, T., Chevrier, V. L. & Jensen, L. D. Surface Area Increase of Silicon Alloys in Li-Ion Full Cells Measured by Isothermal Heat Flow Calorimetry. *J. Electrochem. Soc.* **164**, A2277–A2282 (2017).
- Ming, J. et al. New Insights on Graphite Anode Stability in Rechargeable Batteries: Li Ion
 Coordination Structures Prevail over Solid Electrolyte Interphases. ACS Energy Lett. 3, 335–340
 (2018).
- Cheng, I. F. et al. Synthesis of graphene paper from pyrolyzed asphalt. Carbon 49, 2852–2861
 (2011).
- 21. Cheng, I. F., Xie, Y., Gyan, I. O. & Nicholas, N. W. Highest measured anodic stability in aqueous solutions: graphenic electrodes from the thermolyzed asphalt reaction. *RSC Advances* **3**, 2379 (2013).
- 22. Gyan, I. O., Wojcik, P. M., Aston, D. E., McIlroy, D. N. & Cheng, I. F. A Study of the Electrochemical Properties of a New Graphitic Material: GUITAR. *ChemElectroChem* n/a-n/a (2015) doi:10.1002/celc.201402433.
- 23. Xie, Y. *et al.* Sulfur as an important co-factor in the formation of multilayer graphene in the thermolyzed asphalt reaction. *Journal of Materials Chemistry* **22**, 5723 (2012).
- 24. Kabir, H., Gyan, I., Foutch, J., Zhu, H. & Cheng, I. Application of GUITAR on the Negative Electrode of the Vanadium Redox Flow Battery: Improved V3+/2+ Heterogeneous Electron Transfer with Reduced Hydrogen Gassing. *C* **2**, 13 (2016).
- 25. Gyan, I. O. & Cheng, I. F. Electrochemical study of biologically relevant molecules at electrodes constructed from GUITAR, a new carbon allotrope. *Microchemical Journal* **122**, 39–44 (2015).

- 26. Kabir, H., Gyan, I. O. & Francis Cheng, I. Electrochemical modification of a pyrolytic graphite sheet for improved negative electrode performance in the vanadium redox flow battery. *Journal of Power Sources* **342**, 31–37 (2017).
- 27. Wojcik, P. M. *et al.* Utilizing a Single Silica Nanospring as an Insulating Support to Characterize the Electrical Transport and Morphology of Nanocrystalline Graphite. *Materials* **12**, 3794 (2019).
- 28. Villarreal, C. C., Pham, T., Ramnani, P. & Mulchandani, A. Carbon allotropes as sensors for environmental monitoring. *Current Opinion in Electrochemistry* **3**, 106–113 (2017).
- 29. Radovic, L. R., Karra, M., Skokova, K. & Thrower, P. A. The role of substitutional boron in carbon oxidation. *Carbon* **36**, 1841–1854 (1998).
- 30. Ayala, P., Arenal, R., Rümmeli, M., Rubio, A. & Pichler, T. The doping of carbon nanotubes with nitrogen and their potential applications. *Carbon* **48**, 575–586 (2010).
- 31. Brownlie, L. & Shapter, J. Advances in carbon nanotube n-type doping: Methods, analysis and applications. *Carbon* **126**, 257–270 (2018).
- 32. Stephan, O. *et al.* Doping Graphitic and Carbon Nanotube Structures with Boron and Nitrogen. *Science* **266**, 1683–1685 (1994).
- 33. Villalpando-Paez, F. *et al.* Synthesis and characterization of long strands of nitrogen-doped single-walled carbon nanotubes. *Chemical Physics Letters* **424**, 345–352 (2006).
- 34. Alexander, R. *et al.* In-situ synthesis and densification of boron carbide and boron carbide-graphene nanoplatelet composite by reactive spark plasma sintering. *Ceramics International* **44**, 21132–21137 (2018).
- 35. Kovalčíková, A., Sedlák, R., Rutkowski, P. & Dusza, J. Mechanical properties of boron carbide+graphene platelet composites. *Ceramics International* **42**, 2094–2098 (2016).

- 36. Endo, M., Hayashi, T., Hong, S.-H., Enoki, T. & Dresselhaus, M. S. Scanning tunneling microscope study of boron-doped highly oriented pyrolytic graphite. *Journal of Applied Physics* **90**, 5670–5674 (2001).
- 37. Allardice, D. J. & Walker, P. L. The effect of substitutional boron on the kinetics of the carbon-oxygen reaction. *Carbon* **8**, 375–385 (1970).
- 38. Kuchta, B., Firlej, L., Roszak, S. & Pfeifer, P. A review of boron enhanced nanoporous carbons for hydrogen adsorption: numerical perspective. *Adsorption* **16**, 413–421 (2010).
- 39. Javey, A., Shim, M. & Dai, H. Electrical properties and devices of large-diameter single-walled carbon nanotubes. *Applied Physics Letters* **80**, 1064–1066 (2002).
- 40. Kiang, C.-H. Growth of Large-Diameter Single-Walled Carbon Nanotubes. *The Journal of Physical Chemistry A* **104**, 2454–2456 (2000).
- 41. Mistry, K. S., Larsen, B. A. & Blackburn, J. L. High-Yield Dispersions of Large-Diameter

 Semiconducting Single-Walled Carbon Nanotubes with Tunable Narrow Chirality Distributions. *ACS*Nano 7, 2231–2239 (2013).
- 42. Zhou, W., Ding, L., Yang, S. & Liu, J. Synthesis of High-Density, Large-Diameter, and Aligned Single-Walled Carbon Nanotubes by Multiple-Cycle Growth Methods. *ACS Nano* **5**, 3849–3857 (2011).
- 43. Liu, W. *et al.* Poly(vinyl alcohol) reinforced with large-diameter carbon nanotubes via spray winding. *Composites Part A: Applied Science and Manufacturing* **43**, 587–592 (2012).
- 44. Yang, D. J. et al. Thermal conductivity of multiwalled carbon nanotubes. *Physical Review B* **66**, (2002).
- 45. Kolmogorov, A. N. & Crespi, V. H. Smoothest Bearings: Interlayer Sliding in Multiwalled Carbon Nanotubes. *Physical Review Letters* **85**, 4727–4730 (2000).
- 46. Li, H. J., Lu, W. G., Li, J. J., Bai, X. D. & Gu, C. Z. Multichannel Ballistic Transport in Multiwall Carbon Nanotubes. *Physical Review Letters* **95**, (2005).

- 47. Sharifi, T. *et al.* Nitrogen doped multi walled carbon nanotubes produced by CVD-correlating XPS and Raman spectroscopy for the study of nitrogen inclusion. *Carbon* **50**, 3535–3541 (2012).
- 48. Yudasaka, M., Kikuchi, R., Ohki, Y. & Yoshimura, S. Nitrogen-containing carbon nanotube growth from Ni phthalocyanine by chemical vapor deposition. *Carbon* **35**, 195–201 (1997).
- 49. Seehra, M. S., Geddam, U. K., Schwegler-Berry, D. & Stefaniak, A. B. Detection and quantification of 2H and 3R phases in commercial graphene-based materials. *Carbon* **95**, 818–823 (2015).
- 50. Kim, T.-H. *et al.* Enlarging the d-spacing of graphite and polarizing its surface charge for driving lithium ions fast. *J. Mater. Chem. A* **2**, 7600–7605 (2014).
- 51. Hayes, W. I., Joseph, P., Mughal, M. Z. & Papakonstantinou, P. Production of reduced graphene oxide via hydrothermal reduction in an aqueous sulphuric acid suspension and its electrochemical behaviour. *J Solid State Electrochem* **19**, 361–380 (2015).
- 52. Alam, S. N., Sharma, N. & Kumar, L. Synthesis of Graphene Oxide (GO) by Modified Hummers

 Method and Its Thermal Reduction to Obtain Reduced Graphene Oxide (rGO)*. *Graphene* **06**, 1–18

 (2017).
- 53. Porter, M. Vulcanization of Rubber. in *Organic Chemistry of Sulfur* (ed. Oae, S.) 71–118 (Springer US, 1977). doi:10.1007/978-1-4684-2049-4 3.
- 54. Mukhopadhyay, R., K. De, S. & Chakraborty, S. N. Effect of vulcanization temperature and vulcanization systems on the structure and properties of natural rubber vulcanizates. *Polymer* **18**, 1243–1249 (1977).
- 55. Yudasaka, M. *et al.* Specific conditions for Ni catalyzed carbon nanotube growth by chemical vapor deposition. *Appl. Phys. Lett.* **67**, 2477–2479 (1995).
- 56. Avogadro Free cross-platform molecular editor. Avogadro https://avogadro.cc/.

- 57. Kabir, H. *et al.* The sp2-sp3 carbon hybridization content of nanocrystalline graphite from pyrolyzed vegetable oil, comparison of electrochemistry and physical properties with other carbon forms and allotropes. *Carbon* **144**, 831–840 (2019).
- 58. Chang, C.-C. et al. Strain-induced D band observed in carbon nanotubes. *Nano Research* **5**, 854–862 (2012).
- 59. del Corro, E., Taravillo, M. & Baonza, V. G. Nonlinear strain effects in double-resonance Raman bands of graphite, graphene, and related materials. *Physical Review B* **85**, (2012).
- 60. Mandumpal, J., Gemming, S. & Seifert, G. Curvature effects of nitrogen on graphitic sheets: Structures and energetics. *Chemical Physics Letters* **447**, 115–120 (2007).
- 61. Kim, C. *et al.* Microstructure and Electrochemical Properties of Boron-Doped Mesocarbon Microbeads. *J. Electrochem. Soc.* **147**, 1257 (2000).
- 62. Sheng, Z.-H., Gao, H.-L., Bao, W.-J., Wang, F.-B. & Xia, X.-H. Synthesis of boron doped graphene for oxygen reduction reaction in fuel cells. *J. Mater. Chem.* **22**, 390–395 (2012).
- 63. Kim, Y. A. *et al.* Raman Spectroscopy of Boron-Doped Single-Layer Graphene. *ACS Nano* **6**, 6293–6300 (2012).
- 64. Gebhardt, J. *et al.* Growth and electronic structure of boron-doped graphene. *Phys. Rev. B* **87**, 155437 (2013).
- 65. Wu, Z.-S., Ren, W., Xu, L., Li, F. & Cheng, H.-M. Doped Graphene Sheets As Anode Materials with Superhigh Rate and Large Capacity for Lithium Ion Batteries. *ACS Nano* **5**, 5463–5471 (2011).
- 66. Sahoo, M., Sreena, K. P., Vinayan, B. P. & Ramaprabhu, S. Green synthesis of boron doped graphene and its application as high performance anode material in Li ion battery. *Materials Research Bulletin* 61, 383–390 (2015).

- 67. Ferro, Y., Marinelli, F., Jelea, A. & Allouche, A. Adsorption, diffusion, and recombination of hydrogen on pure and boron-doped graphite surfaces. *The Journal of Chemical Physics* **120**, 11882–11888 (2004).
- 68. Miwa, R. H., Martins, T. B. & Fazzio, A. Hydrogen adsorption on boron doped graphene: an *ab initio* study. *Nanotechnology* **19**, 155708 (2008).



GRAPHICAL ABSTRACT

